Employment of Barkhausen Noise Technique for Assessment of Prestressing Bars Damage with Respect of Their Over-Stressing

František Bahleda [1],*, **Ivan Drevený** [2], **Martin Pitoňák** [1], **Miroslav Neslušan** [3] and **Peter Koteš** [1]

1   Faculty of Civil Engineering, University of Žilina, 010 26 Žilina, Slovakia;
     martin.pitonak@fstav.uniza.sk (M.P.); peter.kotes@uniza.sk (P.K.)
2   Institute of Forensic Research and Education, University of Žilina, 010 26 Žilina, Slovakia;
     ivan.dreveny@usi.sk
3   Faculty of Mechanical Engineering, University of Žilina, 010 26 Žilina, Slovakia;
     miroslav.neslusan@fstroj.uniza.sk
*   Correspondence: frantisek.bahleda@fstav.uniza.sk; Tel.: +421-908-811-973

Abstract: This paper investigates the potential of a non-destructive magnetic technique based on Barkhausen noise emission for the monitoring of prestressing bars with respect to their undesired over-stressing. Barkhausen noise signals are correlated with tensile stress, residual stresses, and microhardness measurements. It was found that prestressing bars exhibit strong magnetic anisotropy which becomes more pronounced along with the increasing degree of the bar's over-stressing. Barkhausen noise emission becomes strongly attenuated in the direction of the tensile stress at the expense of the perpendicular direction. However, the Barkhausen noise emission in the direction of the tensile stress exhibits a continuous and remarkable decrease, whereas the Barkhausen noise steep increase for lower degrees of over-stressing is followed by early saturation for higher over-stressing. This study demonstrates that the Barkhausen noise technique is capable of distinguishing between the prestressing bars loaded below yielding, and those which are over-stressed.

1. Introduction

Prestressing bars represent the high strength low-alloy steels frequently used in civil engineering. These bars are mainly employed for prestressing components during the building of civil constructions, or as a body in those applications in which high load and the corresponding high strength is expected [1,2]. These bars are produced in a variety of dimensions. Moreover, new innovative designs in the beam reinforcement with respect to the bar's shape [3], materials [4], and their corresponding performance have been reported [5]. Loading and repetitive use of prestressing bars is usually carried out in the regime of elastic stresses, well below the yield strength. However, random strong mechanical pulses or heavy loading can result in their over-stressing. Bar over-stressing is strongly undesirable since:

- the bars yielding results in a decrease of prestressing in civil construction and extensive, permanent displacements;
- repetitive use of over-stressed bars should be avoided since bars yielding together with other aspects, such as their fatigue or temperature softening, negatively affects their functional properties [2,6].

For the aforementioned reasons, a fast, reliable method for their monitoring would be beneficial to directly reveal the over-stressed bars during loading in real civil constructions, or in the unloaded state before their further use. Some techniques have already been reported as being suitable for monitoring high strength steels in civil constructions such as ultrasonic tomography [7], gamma rays [8], and electromagnetic testing [9,10].

The low-alloy high strength bars represent the ferromagnetic Fe-alloys with a bcc lattice. Therefore, magnetic techniques could be considered including magnetic Barkhausen noise (MBN). This technique has been employed for monitoring prestressing [11], the corrosion extent [12] and the over-stressing of rope wires [13]. These studies demonstrated the high sensitivity of the MBN technique towards tensile stresses as well as microstructural alterations in these steel wires, being the main load bearing components of the bridges.

MBN occurs in ferromagnetic bodies under alteration of the magnetic field as a result of domains, and the corresponding domain walls (DWs), irreversible, and discontinuous motion. Such motion is a product of the DWs interference with lattice defects (their stress fields) such as dislocation tangles [14–17], grain boundaries [18,19], precipitates [20–22], non-ferromagnetic phases [12], etc. Discontinuous and abrupt jumps of the DWs produces electromagnetic pulses which can be detected on the free surface by using a suitable pick-up coil. Due to interference of the DWs with a variety of lattice defects, MBN signals contain the corresponding information about the microstructure. However, when the superimposed microstructural features pin DWs in motion, their individual contribution to the entire MBN is usually not easy to unwrap. Moreover, besides the microstructure, the stress state also plays a certain role since DW's alignment is driven by exerted stresses as well [23–25].

Loading of the high strength steels in the elastic regime retains an unchanged microstructure and MBN is a function of the stress state only. As soon as the yield strength is exceeded, the superimposed contribution of the microstructure has to be considered as well. The promising potential of MBN for monitoring of prestressing bars with respect of their over-stressing is associated with the high sensitivity of MBN towards the stress state, as well as the microstructure. Therefore, this study investigates the aforementioned field.

The pilot study dealing with rope wires over-stressing has already been reported [13]. Wires exhibit the remarkable preferential matrix orientation along the direction of its length (easy axis of magnetization) and the corresponding decrease of MBN with increasing tensile stresses. Furthermore, MBN evolution during uniaxial tensile stressing can be easily investigated along the wire length only. Prestressing bars preferential orientation is very different with the easy axis of magnetization is close to the axial direction whereas the perpendicular direction along the bar's length represents the hard axis of magnetization. For this reason, evolution of MBN along the bar length remarkably differs from that reported for wires. Moreover, MBN measurements can be executed in the different directions as a result of much higher bars diameter. Therefore, magnetic anisotropy evolution can be investigated in the case of bars as well.

2. Materials and Methods

Over-stressing was carried out on new (unused) prestressing bars made of high strength low-alloy AISI 1050 steel (d = 18 mm, d_a = 21 mm, c = 8 mm, yield strength 950 MPa, measured ultimate strength 1075 MPa, see Figure 1). The chemical composition of the investigated bars is shown in Table 1. The microstructure of the bars is composed of a high tempered martensite, as Figure 2 illustrates. The final shape of the bars, as depicted in Figure 1, is produced by hot rolling followed by subsequent heat treatment to obtain high strength (austenitizing at 1000 °C followed by quenching, tempering at 550 °C and finally their stretching). The surface region is refined as a result of severe plastic deformation during the bar rolling (see Figure 2b).

Table 1. Chemical composition of the investigated bars (wt. %).

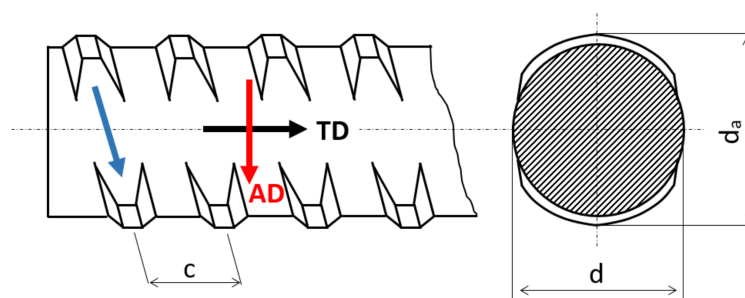| Fe	C	Mn	P	S
Balance	0.55	0.75	<0.04	<0.05

Figure 1. Brief illustration of prestressing bar with indication of MBN measurement directions, (AD—axial direction, TD—transversal direction, c—bar thread lift, d_a – nominal diameter, d – reduced diameter).
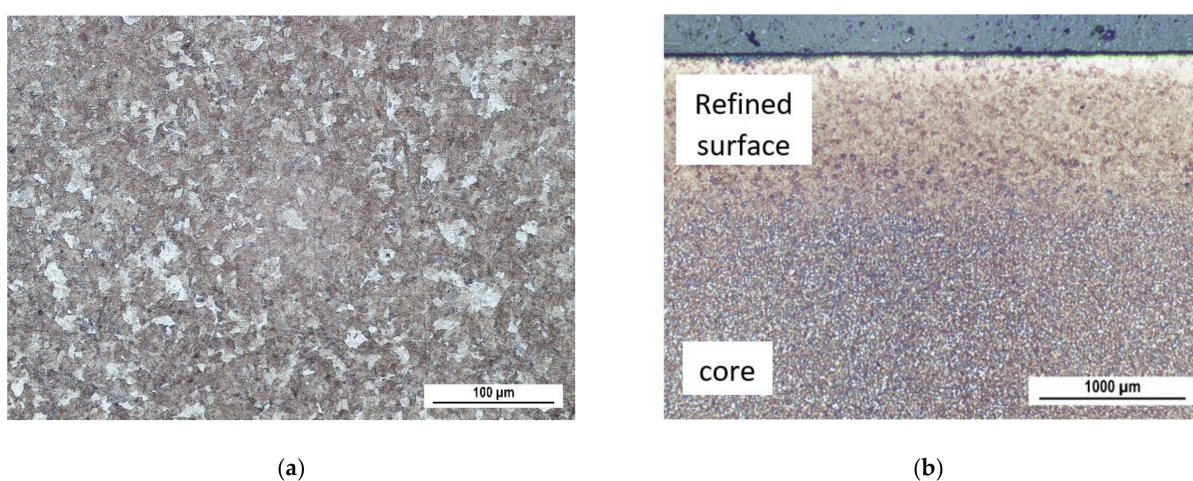

(**a**)   (**b**)

Figure 2. Metallographic images of bar. (**a**) Cross-sectional cut below the refined surface; (**b**) longitudinal cut.

The 280 mm long prestressing bars were loaded by an EU 40 device (Tempos, Opava, The Czech Republic) in three consecutive cycles as follows (see Figures 3 and 4):

- First cycle indicated by blue colour in Figure 4—loading while increasing the tensile stress with the step indicated in Table 2 up to 786 MPa, followed by the progressive release of the tensile stress (indicated by blue color in the figures comparing the stressing cycles).
- Second cycle indicated by black colour in Figure 4—loading while increasing the tensile stress with the step indicated in Table 2 up to 786 MPa, followed by further wire over-stressing controlled by ΔL 5, 10, 15, and 20 mm, holding for 10 s, and finally the progressive release of the tensile stress (indicated by black color in the figures).
- Third cycle indicated by red colour in Figure 4—loading while increasing the tensile stress with the step indicated in Table 2 up to 786 MPa, followed by the progressive release of the tensile stress (indicated by red color in the figures).

Table 2. Stress levels during loading/unloading steps.

Step no.	1	2	3	4	5	6	7	8	9
Stress, MPa	0	98	196	294	393	491	589	688	786

Note: During the stress cycling, after each aforementioned cycle, the bars were not fully unloaded. Three repetitive measurements were carried out for each ΔL.
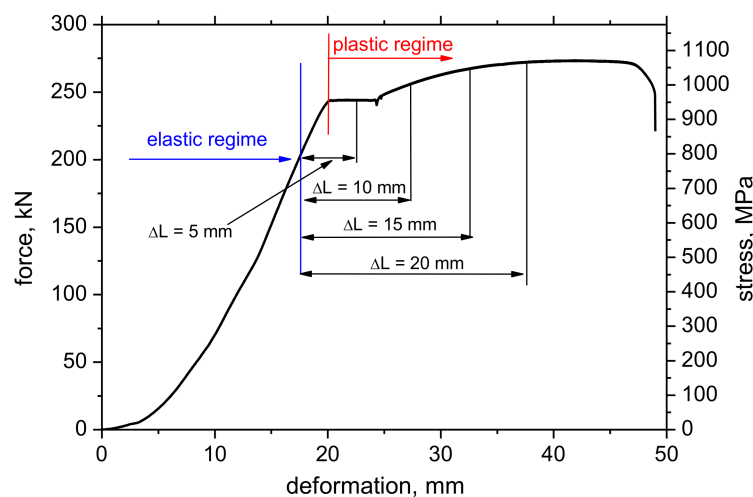
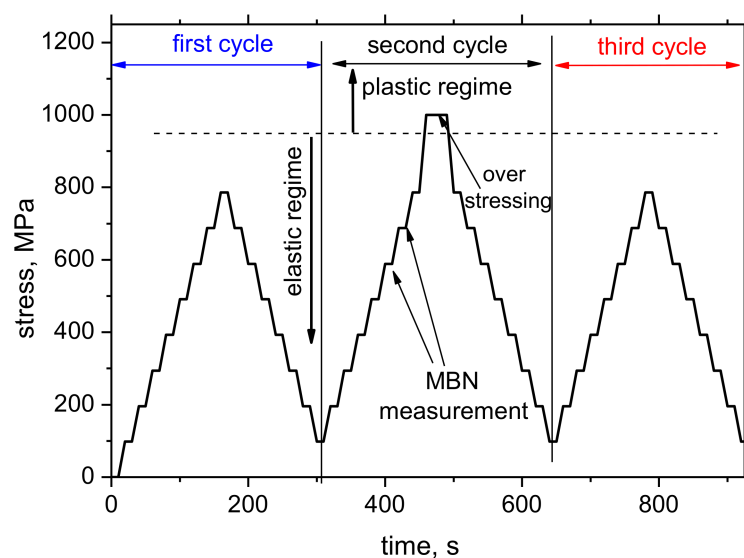**Figure 3.** Engineering stress–strain curve with indicated position of bars over-stressing.

Figure 4. Stress as a function of time during bars loading (10 s holding time for MBN measurements).

The true strains (as well as the true ΔL shown in Figure 3) were measured by the use of the two displacement transducers (HBM WI) due to slipping of the ends of the samples in the EU 40 device clamps. Table 3 summarizes the measured data.

Table 3. Summary of measured data associated with ΔL.

EU 40 ΔL (mm)	True ΔL (mm)—HBM WI	Stress at ΔL (MPa)	Strain at ΔL (%)
0	0	0	0.49
5	1.23	960	0.73
10	5.92	1005	2.62
15	9.75	1050	3.88
20	13.65	1065	5.27
32	21.90	-	10.90

Microhardness (HV0.5) was measured using an Innova Test 400[TM] (Innovatest, Maastricht, The Netherlands) tester by applying a force of 500 g for 10 s on the longitudinal cuts. Microhardness values (as well as the standard deviations) were obtained from five

repeated measurements. The microhardness was measured in the near surface refined region as well as in the deeper core.

To reveal the microstructure of the bars, all bars were cut by use of a Struers Secotom-50 (Struers Inc., Cleveland, USA) in the longitudinal and perpendicular directions. The cut specimens were hot molded, ground, polished, and etched by 3% Nital for 5 s. The hot-molded specimens (longitudinal cuts) were used for measurement of microhardness as well.

Residual stresses after unloading were determined from X-ray diffraction (XRD) patterns acquired using a Proto iXRD Combo diffractometer (Proto manufacturing Ltd., Ontario, Canada). The XRD measurements were performed after the mechanical testing (after the three aforementioned cycles) on the bars surface in the direction of the tensile stress (TD) as well as the axial direction (AD), see Figure 1. The average effective penetration depth of the XRD radiation was approximately 5 μm. Diffraction angles of $2\theta^{hkl}$ were determined at the centre of gravity of diffraction lines $K\alpha_1$ and $K\alpha_2$ of {211} planes of the ferrite phase by the use of Cr-$K\alpha$ radiation. For determination of the residual stress, the Winholtz and Cohen method and the X-ray elastic constants $\frac{1}{2}s_2$ = 5.75 TPa^{-1} and $s_1 = -1.25$ TPa^{-1} were used.

MBN was measured by the use of a RollScan 350 (Stresstech, Jyväskylä, Finland) and analysed with MicroScan 600 (Stresstech, Jyväskylä, Finland) software (magnetizing voltage: 5 V; magnetizing frequency: 125 Hz; MBN pulses in the frequency range of 50–180 kHz; estimated sensing depth: approximately 75 μm, bipolar sensor S1-18-12-01). MBN refers to the *rms* (effective) value of the signal. The bars were magnetised in TD as well as AD. Besides the MBN value, the *PP* (peak position) values were also analysed. *PP* refers to the magnetic field in which the maximum of the MBN envelope is found. MBN measurements were carried out when the samples were in the stressed condition as well as on the fully unloaded samples. Brief illustration of MBN sensor positioning during the measurement in TD is shown in Figure 5 (magnetizing poles were rotated in the sensing head into the perpendicular direction in the case of AD).
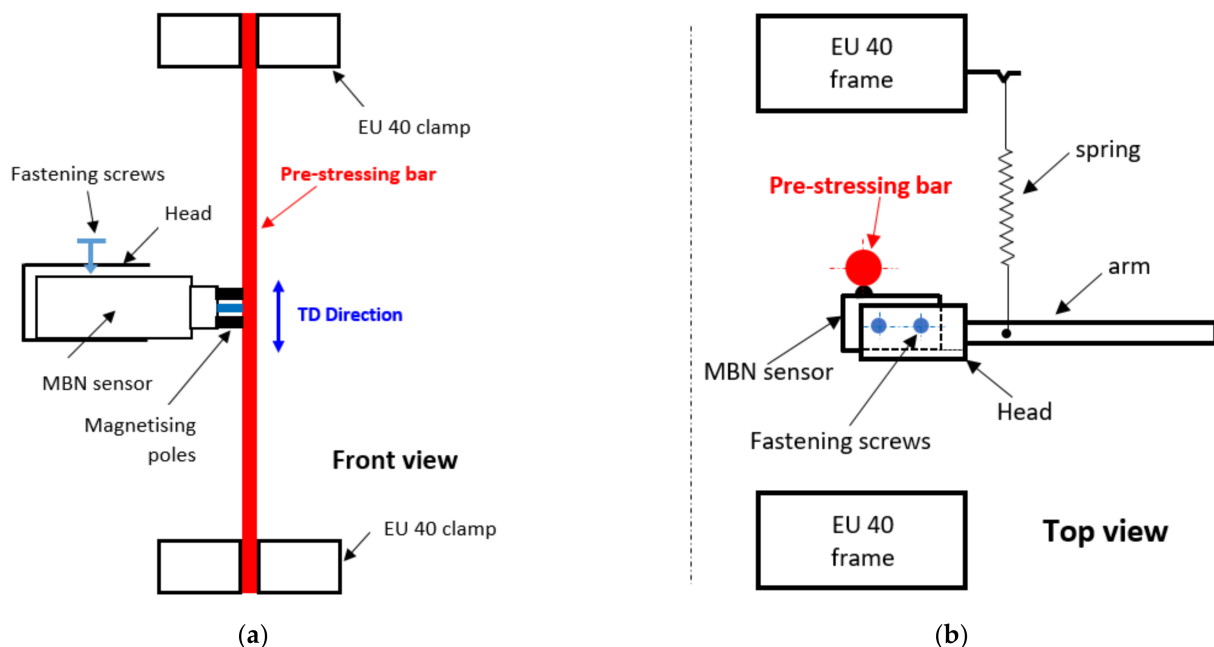

Figure 5. Brief illustration of MBN sensor positioning during prestressing bar loading. (**a**) Front view, (**b**) Top view.

Apart from the bars undergoing the variable degree of over-stressing, the as-received bar, as well as the bar after breakage, were also investigated by the use of MBN and XRD techniques. Moreover, metallographic observation and microhardness measurements were also carried out. The bulk sample corresponds to the $\Delta L = 0$ mm, whereas the fully broken

sample corresponds to the EU 40 ΔL = 32 mm and true ΔL = 21.90 mm, as measured by HBM WI (see Table 3). In the case of the fully broken bar, all measurements and observations were carried out in the necked region (non-homogenous plastic deformation) where plastic instability takes place (at a distance of approximately 5 mm from the broken side). The non-homogenous plastic deformation is associated with the decreasing part of the engineering stress-strain curve beyond its plateau (see Figure 3).

3. Results

3.1. Microhardness and XRD Measurements

Bars yielding initiates permanent matrix alterations, expressed in such terms as residual stresses and/or microhardness. Figure 6a shows that the microhardness growth in the region of homogenous plastic strain is only moderate, followed by a steeper increase in the region of non-homogenous plastic straining (necking). Such behavior is driven by the bar's limited strain hardening and the high ratio between the yield and ultimate strength (0.9) due to attenuated dislocation shearing and a moderate increase in the dislocation density and the corresponding microhardness. Figure 6a illustrates that the initial growth of HV0.5 for the ΔL = 1.23 mm is nearly zero which corresponds with the flat region in stress strain curve (see Figure 3) as a free path region of dislocation motion without interference with other dislocations. As soon as the interrelated dislocation interference takes place, the flat region is replaced by the growth region due to strain hardening and more marked growth in HV0.5. Figure 6a also demonstrates that the surface refined region exhibits a higher HV0.5, but the difference between the surface and deeper core tends to vanish with the bar's increasing over-stressing since the core of lower strength, and the corresponding hardness, consumes more deformation energy as compared with the harder surface. In other words, over-stressing the bars makes strength and hardness more homogenous with respect of their cross section. Finally, it was found that HV0.5 in the core is more than in the refined surface in the region of necking.
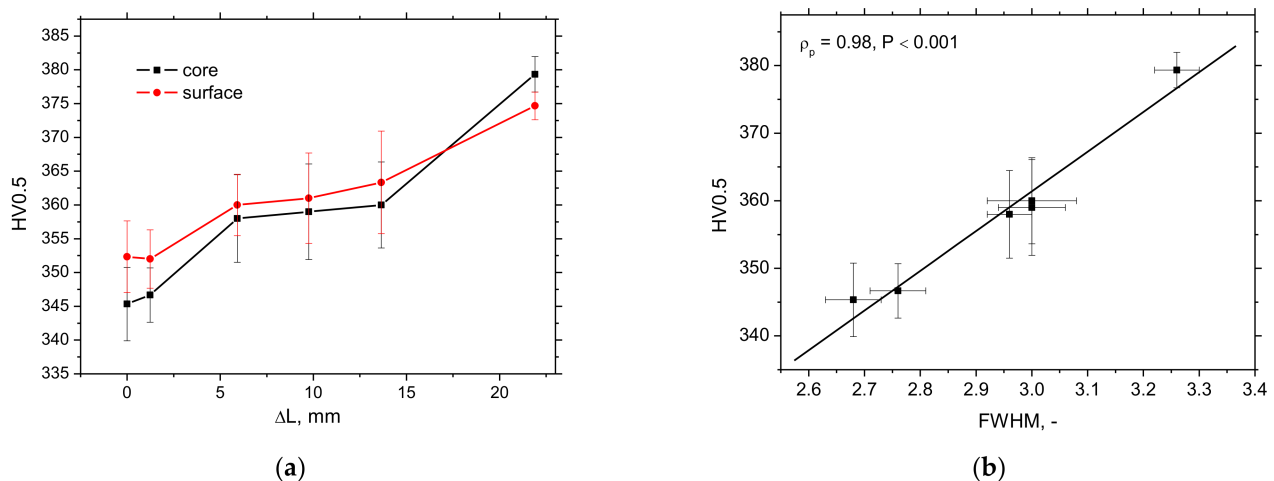

(a)

(b)

Figure 6. Microhardness as a function of ΔL and its correlation with HV0.5. ρ_p refers to the Pearson's correlation coefficient and *p*-value refers to the probability of obtained results. (**a**) Evolution of microhardness, (**b**) microhardness versus FWHM (XRD).

Residual stresses exhibited a progressive decrease during plastic straining and a strong stress anisotropy when the stresses in the TD dominate over the AD (see Figure 7a). XRD measurements indicate that compressive stresses can be found in AD as well as TD. The initial compressive residual stress state is generated during bars production when the bars are heat treated and stretched. Therefore, the compressive stresses for the new bar are about −275 MPa and represent the initial level. The amplitude of compressive residual stress in AD drops down at the expense of the increasing amplitude in TD when the first degree of over-stressing is developed. As soon as the higher degree of over-stressing is

developed, the compressive residual stresses release in TD as well. FWHM extracted from the XRD patterns shows progressive growth (see Figure 7b) and strongly correlates with the microhardness HV0.5 (see Figure 6b). Taking into consideration the limited sensing depth of the XRD technique (about 5 µm), it is clear that the residual stresses and FWHM are associated with the surface region only.
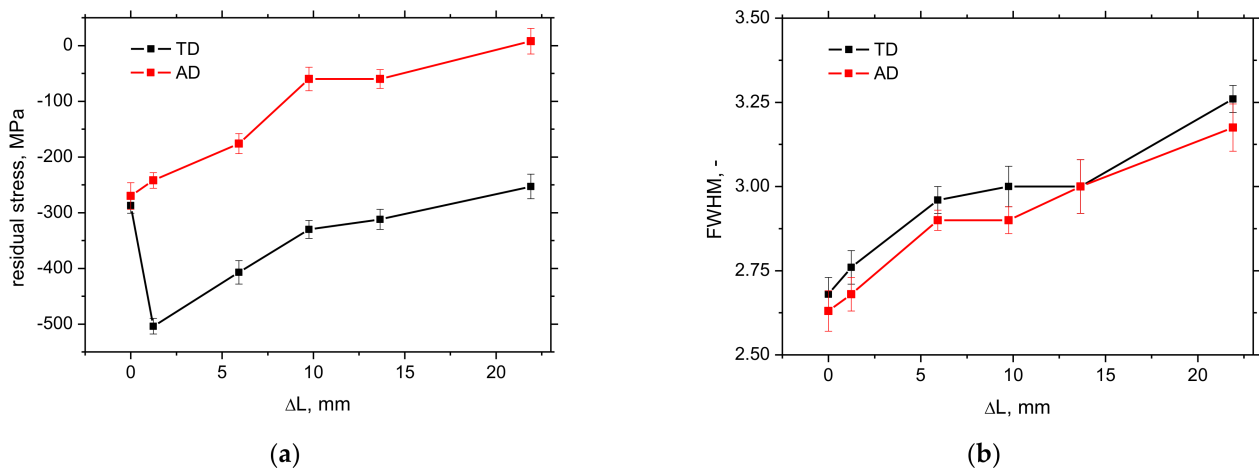

(a)

(b)

Figure 7. Evolution of residual stresses and FWHM as a function of ΔL. (**a**) Residual stresses; (**b**) FWHM.

3.2. MBN Analysis and Metallographic Observations.

Metallographic images presented in Figure 8 (see also Figure 2) reveal no marked preferential matrix orientation. However, it is considered that the easy axis of magnetization, due to the specific DWs alignment, is produced via hot rolling. This easy axis of magnetisation follows the direction of the thread indicated by the blue arrow in Figure 1 (the angle between blue arrow and AD is 23.7°). For this reason, the easy axis of magnetization and the corresponding strongest MBN emission can also be found in this direction. However, due to a shape factor contribution as well as the repetitiveness of MBN measurements, the directions of MBN measurements were carried out in the TD and AD directions (see Figure 1). Note, the shape factor means that the contact between the bar and the sensor in TD is via linear (more or less flat) surface whereas the concave surface due to bars round profile in AD can be found. Therefore, the volume of matrix contributing to MBN emission is slightly different. It is considered that the shape factor gently contributes to the higher MBN in AD as contrasted against TD. The raw MBN signals for the low and high magnitude of tensile stresses in TD are illustrated in Figure 9.
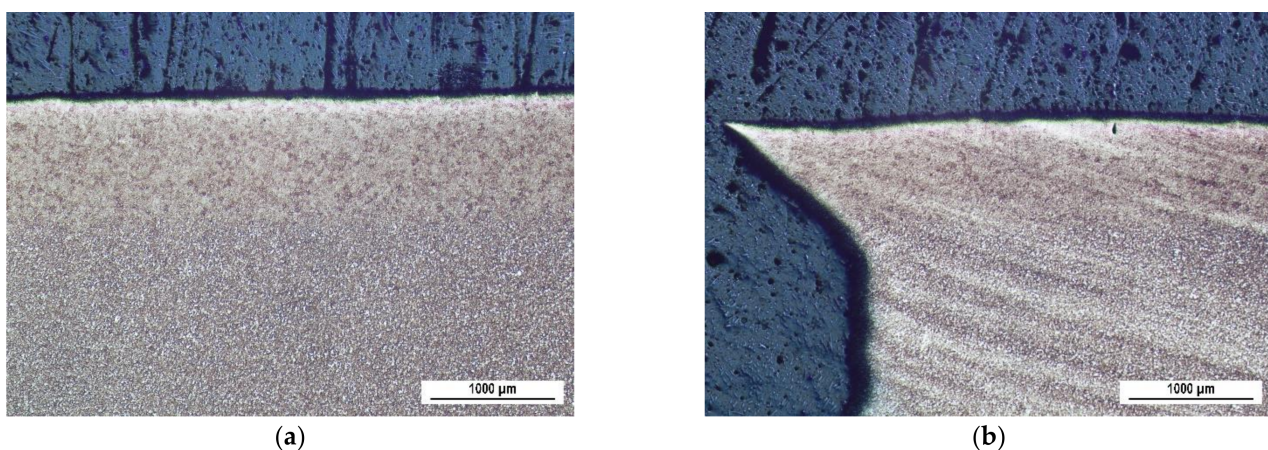

(a)

(b)

Figure 8. Metallographic images—longitudinal cuts. (**a**) ΔL = 13.65 mm, (**b**) ΔL = 21.90 mm.
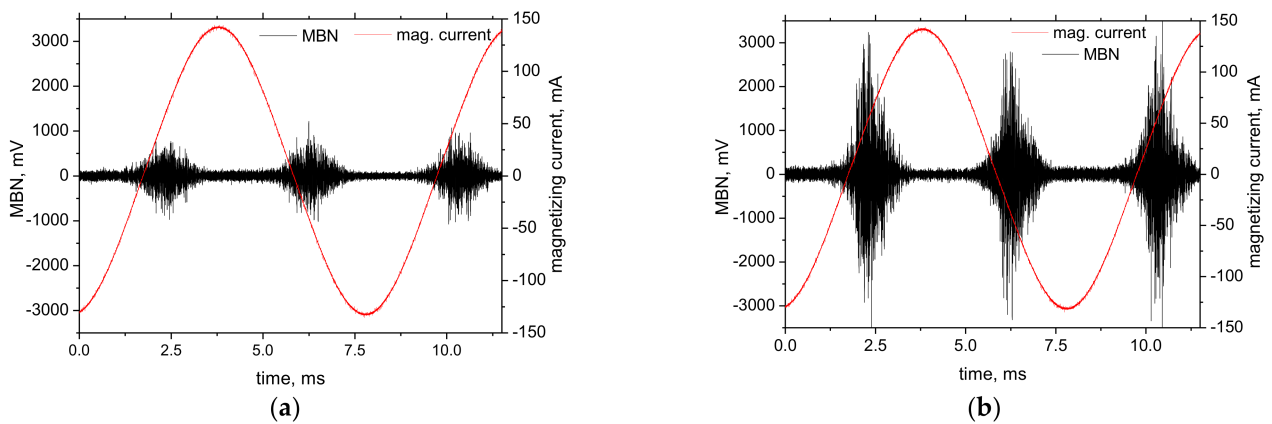
Figure 9. MBN signals for the different magnitude of the tensile stresses, ΔL = 5.92 mm, TD. (**a**) 98 MPa, (**b**) 1005 MPa.

Figures 10–13 illustrate that the AD produces stronger MBN, as compared with the TD, since this direction is aligned closer to the predominating crystallographic orientation. Figure 8 also demonstrates that the remarkable matrix texture produced by dislocations slip can be found in the region of plastic instability (sample necking) beyond the region of the homogenous plastic strains (see Figure 1). Figure 8b clearly depicts shearing bands as a result of the high true stress in the broken end.
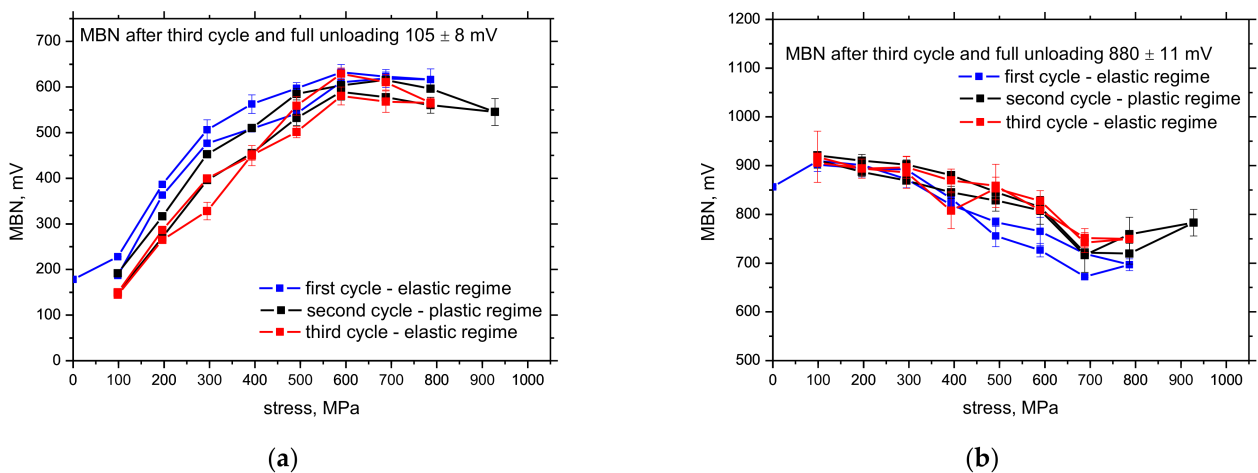

Figure 10. Evolution of MBN during three stress cycles, ΔL = 1.23 mm. (**a**) TD; (**b**) AD.
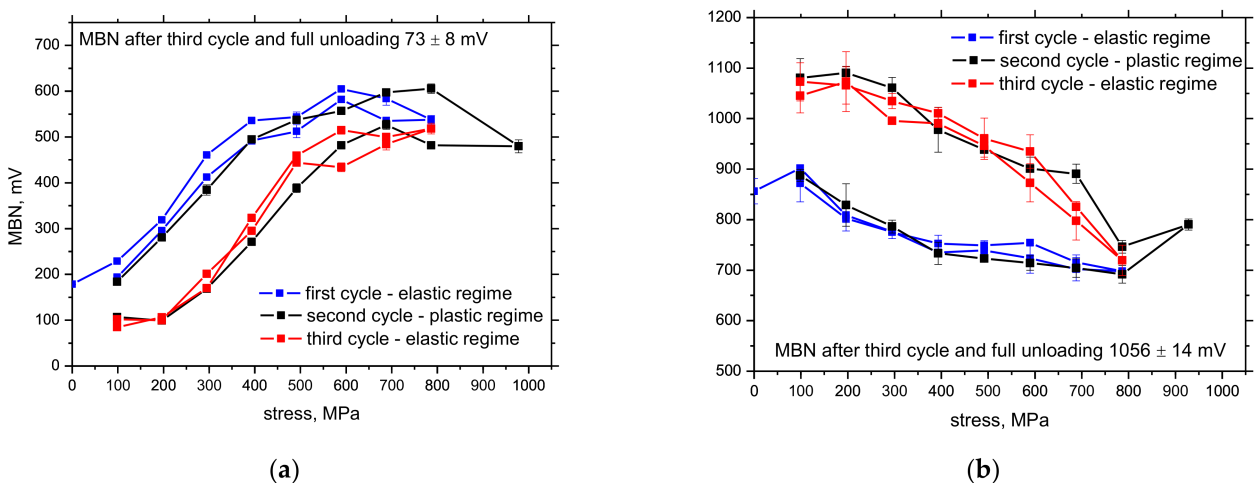

Figure 11. Evolution of MBN during three stress cycles, ΔL = 5.92 mm. (**a**) TD; (**b**) AD.
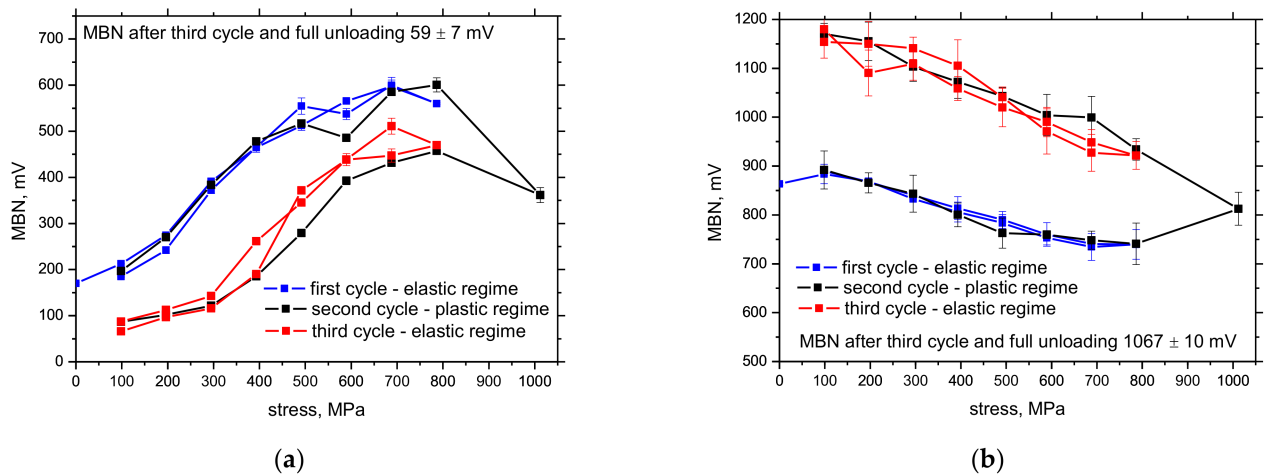
Figure 12. Evolution of MBN during three stress cycles, ΔL = 9.75 mm. (**a**) TD; (**b**) AD.
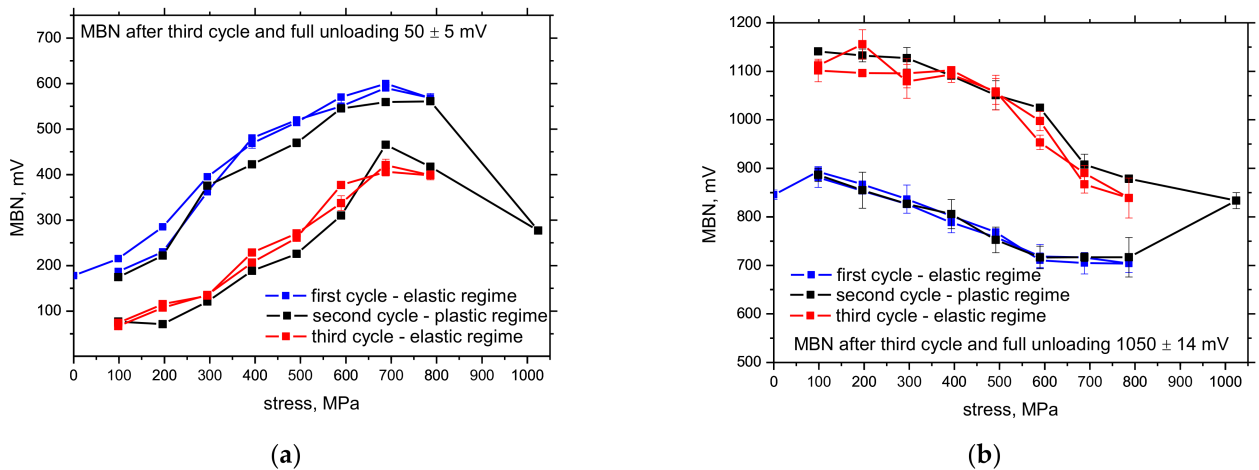

Figure 13. Evolution of MBN during three stress cycles, ΔL = 13.65 mm. (**a**) TD; (**b**) AD.

Tensile stresses are usually associated with an increase of MBN due to the preferential alignment of DW in the direction of the exerted load [23–26]. Figures 10–13 depict that MBN in the TD growth versus stress and saturation can be found for the highest stresses only. On the other hand, this progressive growth is found at the expense of the AD which exhibits a moderate decrease. This behavior is driven by DWs realignment when the DWs tend to follow the direction of uniaxial tensile stress at the expense of the perpendicular direction [23–26]. The progressive growth of MBN versus uniaxial tensile stress indicates that the energy of magneto-crystalline anisotropy E_a is more than the magnetoelastic energy E_σ [26,27]. As soon as E_a is consumed by E_σ, the evolution of MBN-stress curve reaches saturation.

The energy of magnetocrystalline anisotropy for cubic crystals E_a can be calculated by the use of Equation (1) [26,27].

$$E_a = K_1(\alpha_1{}^2\alpha_2{}^2 + \alpha_2{}^2\alpha_3{}^2 + \alpha_1{}^2\alpha_3{}^2) + K_2(\alpha_1{}^2\alpha_2{}^2\alpha_3{}^2) \tag{1}$$

where α_1, α_2, and α_3 are the direction cosines of the magnetisation vector with respect to three cube edges while K_1 and K_2 represent magnetocrystalline anisotropy constants.

The magnetoelastic energy, E_σ, can be calculated by the use of Equation (2) [26,27]

$$E_\sigma = (-3\lambda_s cos^2\varphi)/2 \tag{2}$$

where λ_s is the isotropic magnetostriction and φ defines the angle between the direction of magnetization and the direction of exerted stress σ.

Figures 10–13 also depict that the loading in the elastic region of stresses does not initiate significant alterations of the MBN–stress relationship. As soon as the bars yield and plastic deformation occurs, the evolution of MBN–stress also alters. Figures 10–13 demonstrate that MBN drops down in the TD along with over-stressing, and this drop is permanent at the expense of the growth of MBN in the AD. These figures also show that MBN drops down in the TD and growth in the AD becomes more apparent at the higher degree of over-stressing. The cumulative evolution of ΔMBN in AD and TD beyond the yielding is depicted in Figure 14 (MBN values on the yield strength subtracted, plastic regime only). Figure 15 depicts that the MBN decrease in the TD after full unloading is progressive and monotonous, whereas the AD exhibits a steep initial growth followed by early saturation for higher ΔL. Figures 10–13 also depicts that the alteration of the MBN-stress relationship due to the bar's yielding is permanent. The MBN-stress relationship in the subsequent elastic region of stresses (the third cycle indicated by red color in Figures 10–13) follows the new one generated during the previous phase of the over-stressing (the second cycle indicated by black colour in Figures 10–13). Note, the statement about MBN after third cycle and full unloading (as it is indicated in Figures 10–13) refers to the MBN originated from the samples after over-stressing followed by full tensile stress release (only residual stress state takes role but the external load is equal 0 MPa).
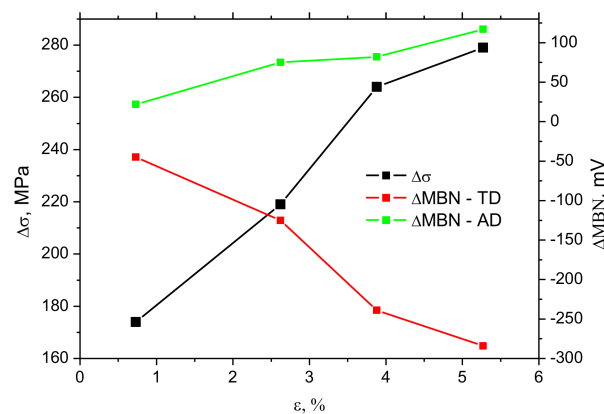

Figure 14. Evolution of ΔMBN and $\Delta\sigma$ during loading beyond the yielding (in the plastic regime only).
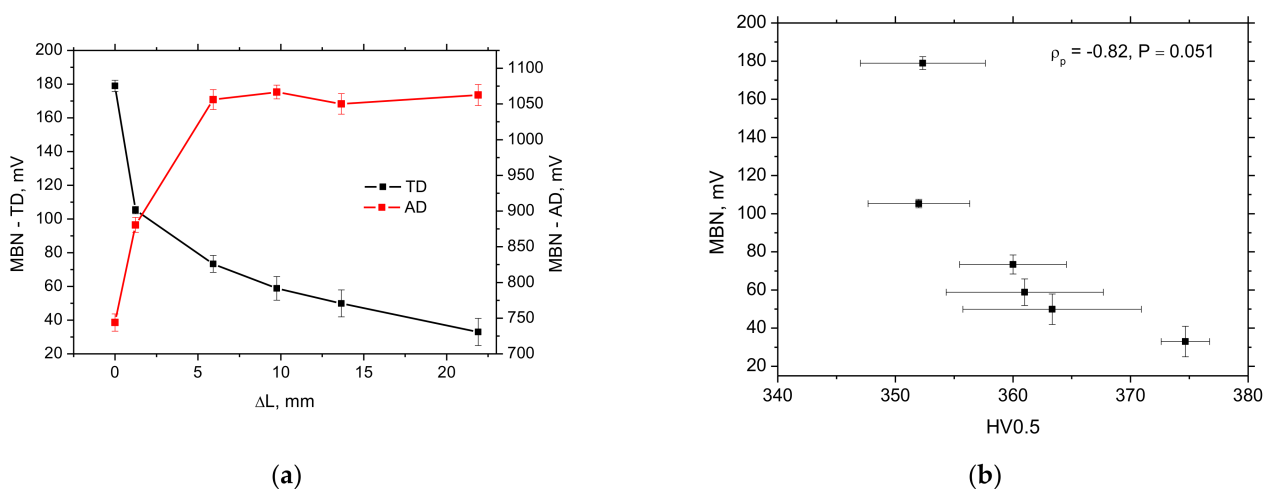

(**a**)

(**b**)

Figure 15. MBN after unloading as a function ΔL and its correlation versus HV0.5. ρ_p refers to the Pearson's correlation coefficient and *p*-value refers to the probability of obtained results. (**a**) MBN as a function of ΔL; (**b**) MBN in TD versus surface HV0.5.

The elastic regime only alters the state of stresses and the microstructure remains unchanged. On the other hand, the plastic regime modifies the bars complexity when the residual stress alterations are superimposed with the microstructural ones. In the elastic regime, the lattice remains more or less unaffected whereas the plastic regime initiates dislocation slip and increases the dislocation density and the corresponding microhardness. Dislocation tangles produce local stress fields in the lattice and increase its pinning strength with respect of the DWs motion. For this reason, MBN in the TD drops down in unloaded samples as compared with the bulk. However, growth of MBN in the AD can be explained by realignment of DWs into this direction during the bar's yielding only. Such behavior has already been reported in other studies [28–30]. The evolution of MBN versus ΔL in the AD, depicted in Figure 15, indicates that the DWs realignment prevails over the increasing pinning strength for the lower ΔL. As soon as their contributions to the MBN become more or less comparable, the evolution of MBN versus ΔL reaches saturation.

Figure 10 shows that alterations of the MBN-stress relationship due to over-stressing is only minor for $\Delta L = 1.23$ mm, as compared with Figures 11–13. Figure 3 depicts that the strain for $\Delta L = 1.23$ mm can be found at the position in the stress-strain curve in which the low strain hardening phase can be found (the flat region beyond the yielding). As soon as more noticeable strain hardening takes place for higher ΔL and the corresponding microstructural alterations becomes more developed, the hysteresis of MBN versus stress during the second (over-stressing) cycle also becomes more apparent.

PP refers to the position in the magnetic field in which an MBN envelope attains the maximum. PP is usually correlated with the magnetic and corresponding mechanical hardness of the investigated matrix [17,31]. Figure 16 illustrates example of MBN envelopes in TD and AD as a function of tensile stress (second cycle). However, Figure 17a (the example of $\Delta L = 9.75$ mm in the AD) depicts no significant contribution of over-stressing to PP. The PP values remain nearly unaffected during the second cycle when the bar yields. Furthermore, the progressive growth of PP along with increasing stress is only gentle. A similar evolution of PP can be found for all ΔL and no noticeable contribution of over-stressing to PP can be found in the TD as well. On the other hand, the fully unloaded samples exhibit continuous growth of PP in the TD until fracture, see Figure 17b. The growth of PP in the TD is a product of increased pinning strength due to increased dislocation density, as expressed in the microhardness HV0.5. The evolution of PP in the AD exhibits:

- a gentle drop for the low ΔL when the contribution of the DWs realignment prevails over the increasing pinning strength of the microstructure;
- followed by nearly constant PP values for medium ΔL when the contribution of the DWs alignment is equally compensated by the increasing pinning strength of the lattice;
- and finally, moderate growth of PP for the highest ΔL when the increasing dislocation density predominates.

It is worth mentioning that MBN originates from the surface refined region only due to its limited skin-depth (taking into consideration the bar's hardness, the estimated skin-depth in this particular case is about 75 μm [32]). Therefore, the correlation analysis between MBN and surface HV0.5 is only reasonable, as Figure 15b illustrates. Figure 15b depicts that MBN in the TD tends to drop down with the microhardness as soon as the strain hardening takes place. MBN shows a marked decrease for $\Delta L = 1.23$ mm as compared with the untouched bulk, whereas HV0.5 does not. On the other hand, the evolution of PP in the TD and HV0.5 is very similar (see Figures 6a, 17b and 18a) and the correlation is very strong, as contrasted with the AD (see Figure 18b).
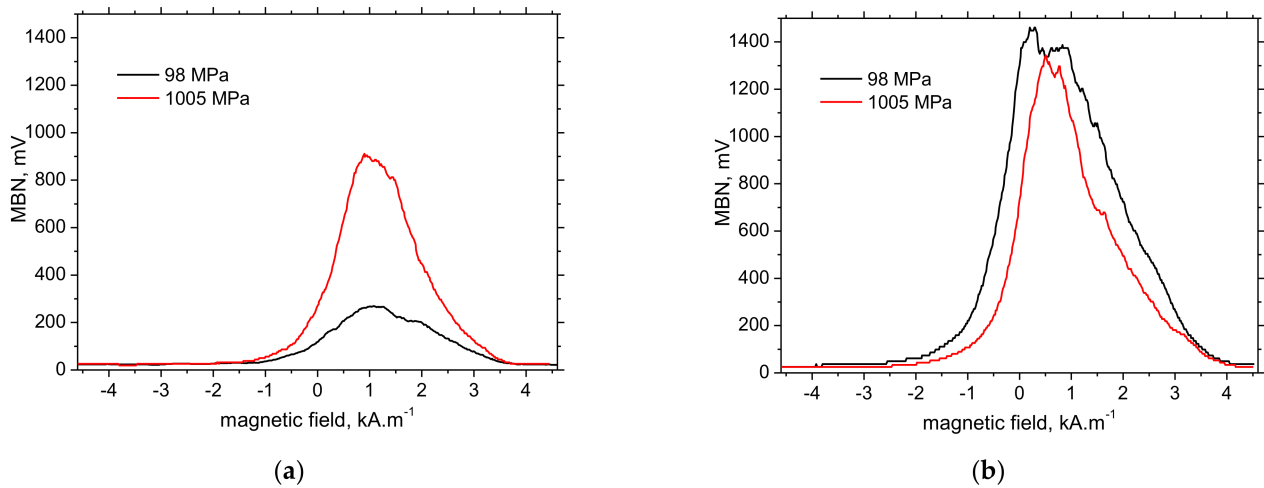
(**a**) (**b**)

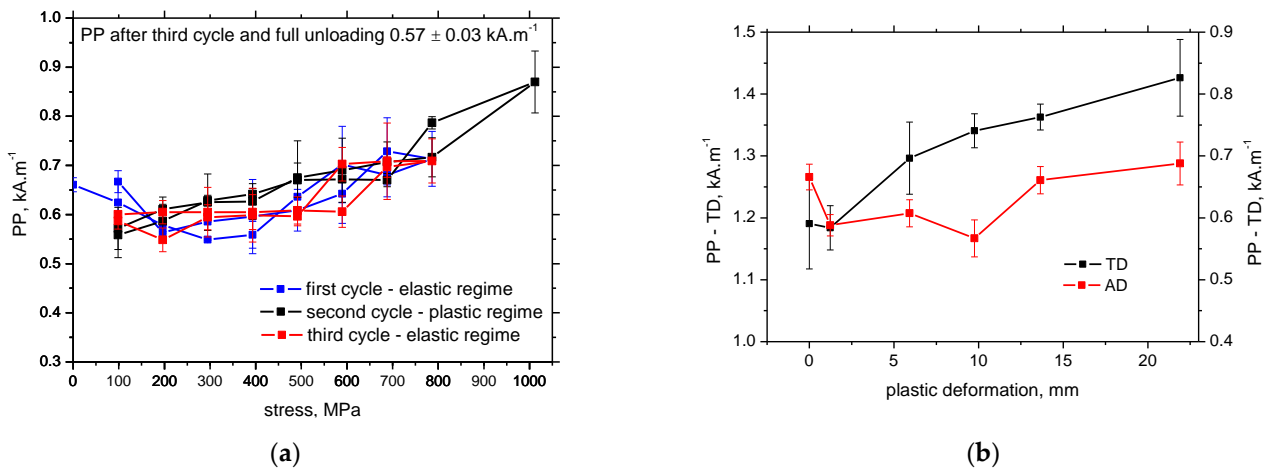**Figure 16.** MBN envelopes for ΔL = 5.92 mm, second cycle. (**a**) TD; (**b**) AD.

(**a**) (**b**)

Figure 17. Evolution of *PP*. (**a**) Evolution of *PP* in AD, ΔL = 9.75 mm; (**b**) *PP* after unloading.
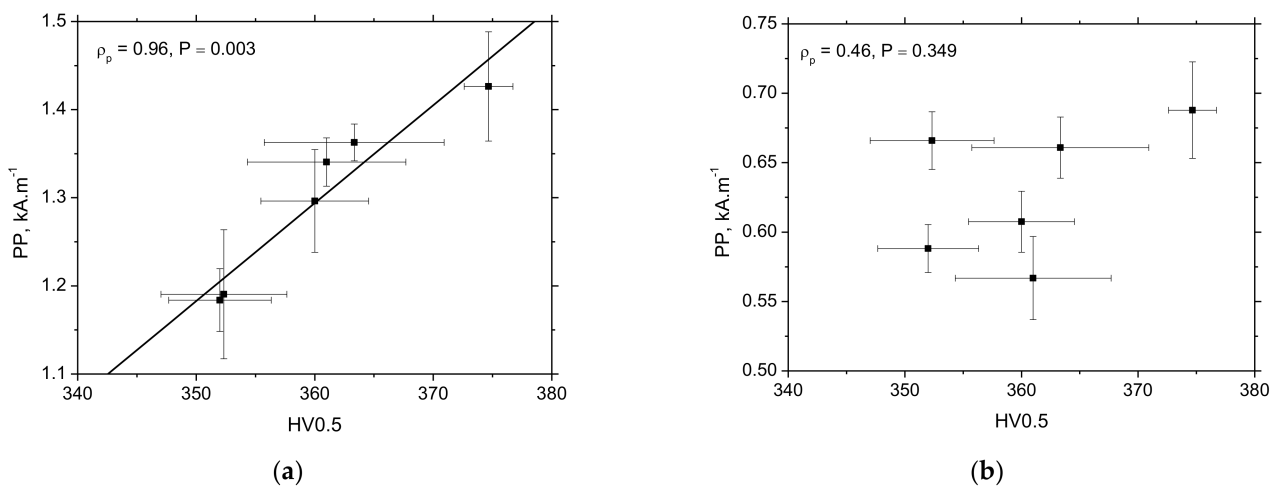

(**a**) (**b**)

Figure 18. Surface microhardness versus *PP* for unloaded bars after plastic straining. (**a**) HV0.5 versus *PP*, TD; (**b**) HV0.5 versus *PP*, AD.

XRD measurements provide information about residual stresses as well as dislocation density expressed in term of FWHM. MBN provides information about DWs motion which is a function of stress state as well as microstructure (expressed in many terms).

Figure 7a demonstrates the decreasing compressive stresses in the TD and the AD as factors contributing to the growth of MBN in the AD [25,30]. However, MBN in the TD drops down despite the decreasing stresses. Furthermore, MBN in the AD exhibits early saturation whereas the residual stresses do not. For these reasons, it is considered that MBN in over-stressed bars is driven mainly by the microstructure (especially the dislocation density), whereas the contribution of the stress state is only minor. Matrix preferential crystallographic (and the corresponding DWs alignment) orientation is close to AD (the easy axis of magnetization) whereas TD represents the hard axis of magnetization. For this reason, the evolutions of MBN after unloading in AD and TD are different, mostly unaffected by residual stress state. The decrease of MBN after unloading in TD is mostly driven by increasing dislocation density (expressed in terms of FWHM and HV0.5) and the corresponding magnetic hardness. On the other hand, the initial grows of MBN in AD is due to superimposing contribution of additional DWs realignment as it was reported earlier [28–30].

Strong correlation between MBN and FWHM can be found in TD only. On the other hand, bar over-stressing and its degree can be linked with the growth of FWHM in both directions as well as decreasing amplitude of residual stress in AD.

4. Conclusions

The findings of this study can be summarized as follows:

- Plot of residual stresses depicts the initial increase in amplitude of compressive residual stresses for TD followed by its progressive decrease whereas release of compressive residual stresses only can be found for AD;
- FWHM of XRD increases with over-stressing and the corresponding degree of plastic deformation for both directions gives information about dislocation density;
- MBN signal shift suggests compressive stress for TD and tensile for AD. However, compressive stresses of decreasing amplitude along with more developed over-stressing were measured in AD as well as TD. This aspect indicates that the contribution of residual stresses with respect of MBN is only minor and the influence of microstructure (and its anisotropy) prevails;
- The high MBN in the TD and the corresponding low MBN in the AD indicate high tensile stress without significant over-stressing;
- Bar over-stressing cannot be detected by the use of MBN directly on the loaded samples since we are unable to distinguish between the MBN for the over-stressed bars and the MBN for bars under a lower magnitude of tensile stress (see Figures 10–13);
- Bar over-stressing can be detected during their unloading at lower tensile stresses when MBN falls below approx. 150 mV in the TD, and/or exceeds 1000 mV in the AD (see Figures 10–13);
- Bars over-stressing and its degree can be linked with the grow of FWHM in both directions as well as decreasing amplitude of residual stress in AD;
- Decreasing MBN in the TD obtained from the unloaded bars (as compared with the bulk) can be linked with the increasing degree of their over-stressing, whereas the high MBN in the AD provides information about the bar's yielding, but the sensitivity towards the degree of over-stressing is limited (see Figure 15).

Author Contributions: Conceptualization, F.B. and I.D.; Methodology, M.N. and M.P.; Software, M.N. and P.K.; Validation, F.B. and M.P.; Formal analysis, M.P. and I.D.; Investigation, F.B., M.N., I.D. and M.P.; Resources, F.B. and P.K.; Data curation, P.K.; Writing—original draft preparation, F.B. and I.D.; Writing—review and editing, F.B. and I.D.; Visualization, M.P. and P.K.; Supervision, F.B. and M.P.; Project administration, F.B. and I.D.; Funding acquisition, F.B. and P.K. All authors have read and agreed to the published version of the manuscript.

2014–2020 of the project: Innovative Solutions for Propulsion, Power and Safety Components of Transport Vehicles, code ITMS 313011V334, co-financed by the European Regional Development Fund.

Institutional Review Board Statement: Not applicable.

Data Availability Statement: The raw data required to reproduce these findings cannot be shared easily due to technical limitations (especially MBN raw signals are too large due to very high sampling frequency). However, authors can share the data on any individual request (please contact the corresponding author by the use of its mailing address.

Conflicts of Interest: The authors declare no conflict of interest.

References

1. Yang, K.H.; Mun, J.H.; Hwang, S.H. Cyclic shear behaviour of masonry walls strengthened with pre-stressed bars and glass fibre grids. *Comp. Struct.* **2020**, *238*, 111961. [CrossRef]
2. Zhong, X.; Zhang, T.; Zhao, C.; Shu, X.; Shen, M.; Chen, Y.F. New non-destructive dynamic tensile testing of prestressing fine-rolled screw-threaded steel bars. *Eng. Struct.* **2019**, *182*, 153–163. [CrossRef]
3. Li, X.; Wu, Z.; Zheng, J.; Cao, Q. Rate-dependent bond performance of plain bars in concrete under biaxial transverse tensions. *Eng. Struct.* **2020**, *216*, 110740. [CrossRef]
4. Said, M.; Shanour, A.S.; Mustafa, T.; Abdel-Kareem, A.H.; Khalil, M.M. Experimental flexural performance of concrete beams reinforced with an innovative hybrid bars. *Eng. Struct.* **2021**, *226*, 111348. [CrossRef]
5. Gao, D.; Gu, Z.; Tang, J. Fatigue performance and stress range modeling of SFRC beams with high-strength steel bars. *Eng. Struct.* **2020**, *216*, 110706. [CrossRef]
6. Hou, X.; Zheng, W.; Kodur, V.; Sun, H. Effect of temperature on mechanical properties of prestressing bars. *Constr. Build. Mater.* **2014**, *61*, 24–32. [CrossRef]
7. Martin, J.; Broughton, K.J.; Giannopolous, A. Ultrasonic tomography of grouted duct post-tensioned reinforced concrete bridge beams. *NDT & E Int.* **2001**, *34*, 107–113. [CrossRef]
8. Peng, P.-C.; Wang, C.-Y. Use of gamma rays in the inspection of steel wire ropes in suspension bridges. *NDT E Int.* **2015**, *75*, 80–86. [CrossRef]
9. Christen, R.; Bergamini, A.; Motavalli, M. Influence of steel wrapping on magneto-inductive testing of the main cables of suspension bridges. *NDT E Int.* **2009**, *42*, 22–27. [CrossRef]
10. Cao, Y.N.; Zhang, D.L.; Xu, D.G. The state-of-art of quantitative testing of wire rope. *Nondestruct. Test.* **2005**, *27*, 91–95.
11. Neslušan, M.; Bahleda, F.; Moravčík, M.; Zgútová, K.; Pastorek, F. Assessment of tendon prestressing after long term operation via Barkhausen noise technique. *Materials* **2019**, *12*, 3450. [CrossRef]
12. Neslušan, M.; Bahleda, F.; Minárik, P.; Zgútová, K.; Jambor, M. Non-destructive monitoring of corrosion extent in steel rope wires via Barkhausen noise emission. *J. Magn. Magn. Mater.* **2019**, *484*, 179–187. [CrossRef]
13. Neslušan, M.; Bahleda, F.; Trojan, K.; Pitoňák, M.; Zgútová, K. Barkhausen noise in over-stressed wires. *J. Magn. Magn. Mater.* **2020**, *513*, 167134. [CrossRef]
14. Fiorillo, F.; Küpferling, M.; Appino, C. Magnetic Hysteresis and Barkausen Noise in Plastically Deformed Steel Sheets. *Metals* **2017**, *8*, 15. [CrossRef]
15. Kleber, X.; Vincent, A. On the role of residual internal stresses and dislocations on Barkhausen noise in plastically deformed steel. *NDT E Int.* **2004**, *37*, 439–445. [CrossRef]
16. Piotrowski, L.; Chmielewski, M.; Kowalewski, Z.L. The Dominant Influence of Plastic Deformation Induced Residual Stress on the Barkhausen Effect Signal in Martensitic Steels. *J. Nondestruct. Eval.* **2017**, *36*, 10. [CrossRef]
17. Piotrowski, L.; Augustyniak, B.; Chmielewski, M.; Kowalewski, Z. Multiparameter analysis of the Barkhausen noise signal and its application for the assessment of plastic deformation level in 13HMF grade steel. *Meas. Sci. Technol.* **2010**, *21*, 115702. [CrossRef]
18. Neslušan, M.; Minárik, P.; Grenčík, J.; Trojan, K.; Zgútová, K. Non-destructive evaluation of the railway wheel surface damage after long-term operation via Barkhausen noise technique. *Wear* **2019**, *420–421*, 195–206. [CrossRef]
19. Ktena, A.; Hristoforou, E.; Gerhardt, G.J.; Missell, F.P.; Landgraf, F.J.; Rodrigues, D.L.; Alberteris-Campos, M. Barkhausen noise as a microstructure characterization tool. *Phys. B* **2014**, *435*, 109–112. [CrossRef]
20. Anglada-Rivera, J.; Padovese, L.R.; Capó-Sanchez, J. Magnetic Barkhausen noise and hysteresis loop in commercial carbon steel: Influence of applied tensile stress and grain size. *J. Magn. Magn. Mater.* **2001**, *231*, 299–306. [CrossRef]
21. Neslušan, M.; Minárik, P.; Čilliková, M.; Kolařík, K.; Rubešová, K. Barkhausen noise emission in tool steel X210Cr12 after semi-solid processing. *Mater. Charact.* **2019**, *157*, 109891. [CrossRef]
22. Jarrahi, F.; Kashefi, M.; Ahmadzade-Beiraki, E. An investigation into the applicability of Barkhausen noise technique in evaluation of machining properties of high carbon steel parts with different degrees of spheroidization. *J. Magn. Magn. Mater.* **2015**, *385*, 107–111. [CrossRef]
23. Liu, J.; Tian, G.Y.; Gao, B.; Zeng, K.; Zheng, Y.; Chen, J. Micro-macro characteristics between domain wall motion and magnetic Barkhausen noise under tensile stress. *J. Magn. Magn. Mater.* **2020**, *493*, 165719. [CrossRef]

24. Sorsa, A.; Santa-Aho, S.; Wartiainen, J.; Suominen, L.; Vippola, M.; Leiviskä, K. Effect of Shot Peening Parameters to Residual Stress Profiles and Barkhausen Noise. *J. Nondestruct. Eval.* **2018**, *37*, 10. [CrossRef]
25. Karpuschewski, B.; Bleicher, O.; Beutner, M. Surface Integrity Inspection on Gears Using Barkhausen Noise Analysis. *Procedia Eng.* **2011**, *19*, 162–171. [CrossRef]
26. Jiles, D. *Introduction to Magnetism and Magnetic Materials*, 3rd ed.; Taylor & Francis Group: New York, NY, USA, 2016.
27. Chikazumi, S. *Physics of Ferromagnetism*, 2nd ed.; Oxford University Press: Oxford, UK, 2005.
28. Roskosz, M.; Fryczowski, K.; Schabowicz, K. Evaluation of Ferromagnetic Steel Hardness Based on an Analysis of the Barkhausen Noise Number of Events. *Materials* **2020**, *13*, 2059. [CrossRef]
29. Lindgren, M.; Lepistö, T. Effect of prestraining on Barkhausen noise vs. stress relation. *NDT & E Int.* **2001**, *34*, 337–344. [CrossRef]
30. Neslušan, M.; Jurkovič, M.; Kalina, T.; Pitoňák, M.; Zgútová, K. Monitoring of S235 steel over-stressing by the use of Barkhausen noise technique. *Eng. Fail. Anal.* **2020**, *117*, 104843. [CrossRef]
31. Sorsa, A.; Leiviskä, K.; Santa-Aho, S.; Lepistö, T. Quantitative prediction of residual stress and hardness in case-hardened steel based on the Barkhausen noise measurement. *NDT & E Int.* **2012**, *46*, 100–106. [CrossRef]
32. Stupakov, A.; Perevertov, A.; Neslušan, M. Reading depth of the magnetic Barkhausen noise. I. One-phase semi-hard ribbons. *J. Magn. Magn. Mater.* **2020**, *513*, 167086. [CrossRef]